HDL TR-1705

AD-A014891

ANALYTICAL INVESTIGATION OF INDUCTIVE LOOP COUPLING FOR REMOTE SET FUZING

June 1975

U.S. Army Materiel Command
HARRY DIAMOND LABORATORIES
Adelphi, Maryland 20783

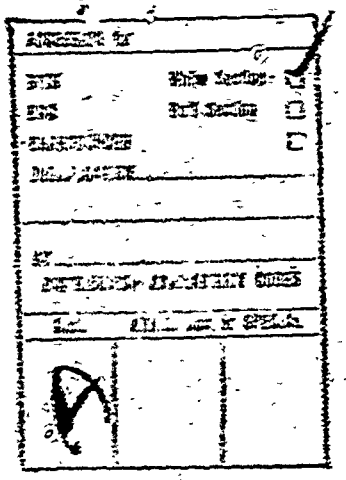

The findings in this report are not to be construed as an official Department of the Army position unless so designated by other authorized documents.

Citation of manufacturers' or trade names does not constitute an official indorsement or approval of the use thereof.

Destroy this report when it is no longer needed. Do not return it to the originator.

UNCLASSIFIED

SECURITY CLASSIFICATION OF THIS PAGE (When Data Entered)

REPORT DOCUMENTATION PAGE	READ INSTRUCTIONS BEFORE COMPLETING FORM
1. REPORT NUMBER: HDL-TR-1705	2. GOVT ACCESSION NO. / 3. RECIPIENT'S CATALOG NUMBER
4. TITLE (and Subtitle): Analytical Investigation of Inductive Loop Coupling for Remote Set Fuzing.	5. TYPE OF REPORT & PERIOD COVERED: Technical Report. / 6. PERFORMING ORG. REPORT NUMBER
7. AUTHOR(s): Albert J. Sambuco	8. CONTRACT OR GRANT NUMBER(s): DA-1W362301A20700 H2-AZ-441
9. PERFORMING ORGANIZATION NAME AND ADDRESS: Harry Diamond Laboratories, 2800 Powder Mill Road, Adelphi, MD 20783	10. PROGRAM ELEMENT, PROJECT, TASK AREA & WORK UNIT NUMBERS: Prog. Element - 6.23.01.A
11. CONTROLLING OFFICE NAME AND ADDRESS: Commander, USA Armaments Command, Rock Island, IL 61201	12. REPORT DATE: June 1975 / 13. NUMBER OF PAGES: 30 (12) 22p
14. MONITORING AGENCY NAME & ADDRESS (if different from Controlling Office)	15. SECURITY CLASS. (of this report): UNCLASSIFIED / 15a. DECLASSIFICATION/DOWNGRADING SCHEDULE

16. DISTRIBUTION STATEMENT (of this Report)

Approved for Public Release; Distribution Unlimited

17. DISTRIBUTION STATEMENT (of the abstract entered in Block 20, if different from Report)

18. SUPPLEMENTARY NOTES

HDL Project No. - A22444
Pron. No. - A145275101
AMCMS Code - 612301.11.17500

Also sponsored by AMC

19. KEY WORDS (Continue on reverse side if necessary and identify by block number)

Inductive loop coupling
Remote set fuzing

20. ABSTRACT (Continue on reverse side if necessary and identify by block number)

A simplified equivalent-circuit model has been developed to describe the inductive coupling utilized in a remote set fuzing application. Actual measurements have confirmed that this circuit can be used to predict performance of changed physical parameters. An outline of a technique for obtaining an exact solution is also presented.

DD FORM 1 JAN 73 1473 EDITION OF 1 NOV 65 IS OBSOLETE

UNCLASSIFIED

SECURITY CLASSIFICATION OF THIS PAGE (When Data Entered)

TABLE OF CONTENTS

LIST OF ILLUSTRATIONS

LIST OF ILLUSTRATIONS (CONT'D)

1. INTRODUCTION

1.1 Background

An experimental investigation by the Harry Diamond Laboratories (HDL) has shown the feasibility of inductive loop coupling for remote set fuzing.* This was accomplished by feeding an ac signal into a "sending" coil wrapped around the body of an LAU6IA Rocket Launcher and noting the signal level at the output of a "receiving" coil wrapped around the base of an M429 fuze that was mounted on a 2.75-in. rocket warhead in one of the rocket tubes. By introducing axial slots in the rocket tube and the fuze base, the resulting output was sufficient to provide primary power and a coded (fuze-mode setting) signal to operate the fuze circuitry.

Since there is considerable interest in the remote-set concept, an analytical investigation was undertaken to

(1) find an equivalent circuit electrical model of the inductively-coupled remote set design which could be used to verify the observed performance, and

(2) aid in prediction of the effects of configuration changes on the receiving coil output voltage.

Two approaches to the problem of describing a model were considered. One was to propose an equivalent electrical circuit from a study of the physical configuration, and then attempt to verify the resulting proposed model by using measurement techniques (see app A for measurement details). A second possible approach is to describe the physical configuration in terms of boundary conditions of Maxwell's equations and obtain the solutions. The former, empirical, approach was selected. The second approach, although more general, is not timely and practical at this writing. In the future, a more rigorous solution may be desired; thus, the problem has been defined by Orval Cruzan in appendix B.

The portion of the rocket launcher system selected for analysis was a slotted, aluminum rocket tube with the sending coil wound around the tube and over the slot, and a slotted aluminum model of an M429 fuze base with a receiving coil wound around it and over its slot. This configuration is shown in figure 1.

The equivalent circuit postulated was a link-coupled circuit[1] (see fig. 2) where the sending coil was the primary circuit, the aluminum rocket tube was represented by a link coupling coil, and the

*This investigation was made by Edward T. Spielman at the Harry Diamond Laboratories in 1973.

[1] Frederick E. Terman, Radio Engineers Handbook (McGraw-Hill, N.Y. 1943), p. 128.

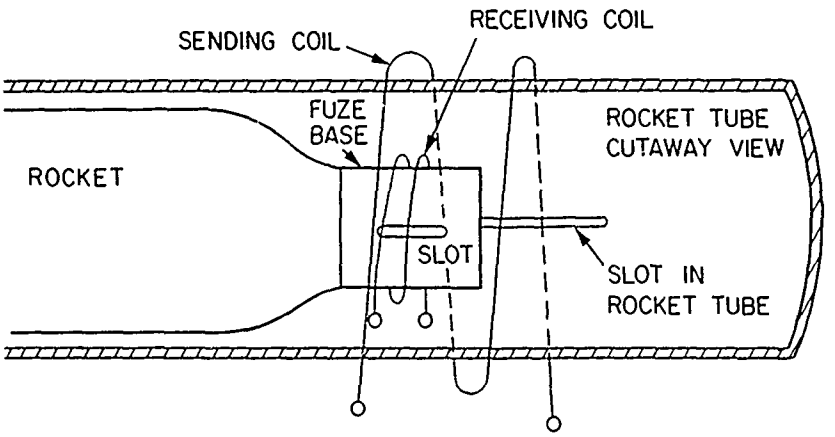

Figure 1. Basic inductive coupled physical configuration (cutaway view).

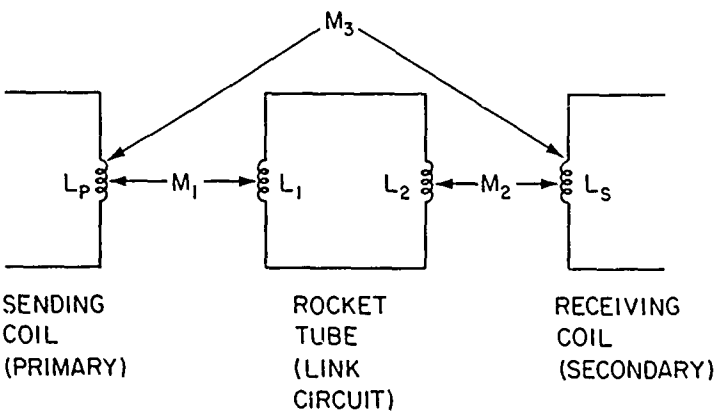

Figure 2. Basic equivalent circuit.

receiving coil was the secondary circuit. (Electrically non-conducting rocket launcher tubes, such as paper used in the LAU-3 launcher family, or corner-drawn fiber glass developed by the Naval Surface Weapons Center, formerly the Naval Ordnance Laboratory, would obviate the link circuit, and the simpler primary and secondary winding equivalent circuit can be used.[2]) This three-coil circuit was further reduced to a more conventional primary and secondary equivalent circuit with inductive mutual coupling. The circuit elements of the reduced coupled

[2]*Joint Munitions Effectiveness Manual, Air-to-Surface Weapons Characteristics Handbook (JMEM) Change 5, 29 December 1972 (Confidential).*

circuit were determined experimentally and verified to within reasonable values. The equivalent circuit thus developed can be used

(1) to explain the inductive coupling operation, and

(2) in combination with empirically derived functions as a design aid.

Thus, the stated objectives of the report were substantially realized.

1.2 Summary

An experimental design demonstrating the ability to remotely select one of several fuze modes (i.e., PD, proximity or time) by inductive coupling was analyzed. The configuration analyzed was a sending coil wound around a 3-in.-diameter aluminum rocket tube for a 2.75-in. rocket warhead, and a receiving coil wound around the aluminum base of an M429 fuze mounted in a 2.75-in. rocket warhead.

Ordinarily, the signal strength with the configuration described would be impracticable because of the shielding effect of the rocket tube intervening between the two windings. The addition of slots under the coils, in the rocket tube, and in the warhead base makes the inductive coupling concept practicable. The analysis was accomplished by proposing and verifying an equivalent three-winding tandem-coupled circuit (where the rocket tube was represented by the intermediate "link" circuit). The proposed equivalent circuit was obtained from consideration of electromagnetic field theory principles. The equivalent three-winding circuit was then reduced to a two winding equivalent circuit using circuit theory techniques. Electronic measurement techniques were then applied to obtain the component values of the equivalent circuit from the physical configuration.* Verification of the model was accomplished by finding the coupling coefficient "M" to be constant over a wide frequency range where the output voltage was maximized by using different external capacitors to resonate the output circuit. Then, using the value of M thus determined, the frequency response of the circuit was measured with a fixed value of output capacitance. The resulting frequency response obtained was found to be within instrument accuracy of that predictable from the assumed equivalent circuit. It was determined that the equivalent circuit developed could be used as a qualitative aid in understanding the effects of external circuit changes on the voltage transfer characteristics. The limitation of the approach used is that it cannot be directly used to create a paper design. Further work

Measurement techniques are presented in appendix A.

would be necessary to obtain empirical curves that would describe the effects of physical configuration changes (e.g., wire size, size and number of slots, relative axial position of sending and receiving coils, etc). A purely theoretical approach was outlined using a theoretic-numeric technique for the simple case of a single rocket tube with idealized parameters. The additional complexity of this theoretical method, when considering possible effects of adjacent rocket tubes, suggests that the equivalent circuit technique (wherein the effects of adjacent rocket tubes are included in the measurement) is the better approach at present.

2. PROPOSED MODEL

A simplified equivalent circuit of the basic physical configuration in figure 1 is shown as the circuit in figure 3, where the primary circuit represents the sending coil, the intermediate or link circuit represents the rocket tube, and the secondary circuit represents the receiving coil.

C_P and C_S represent the stray capacitances across the sending and receiving coils, respectively. The "conducting-shield"[1] effect of the rocket tube results in a negligible value for M_3, as explained further in section 4, so that M_3 can be neglected as a first-order approximation. M_1 is the inductive coupling factor from sending coil to rocket tube, and M_2 represents the inductive coupling between the rocket tube slot and the receiving coil. Measurements of the magnitude of resistance reflected from the rocket tube are below the accuracy of the instrumentation so that R_T, which represents the finite conductivity of the rocket tube, can be neglected. The simplified equivalent circuit with these approximations is shown in figure 4.

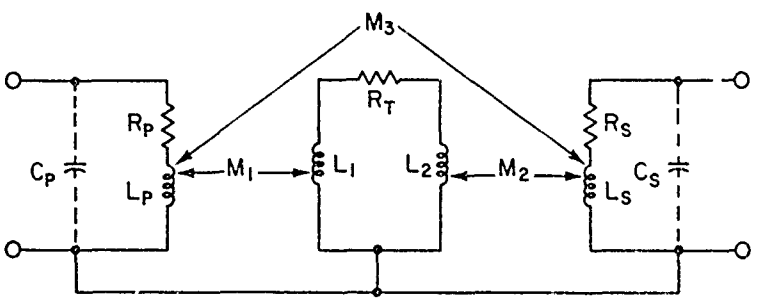

Figure 3. Equivalent electrical circuit model.

---

[1] *Frederick E. Terman, Radio Engineers Handbook (McGraw-Hill, N.Y. 1943), p. 128.*

Finally, the circuit in figure 4 can be reduced to a working analytical model from which measurements of the proposed circuit elements can be made and from which the model can be exercised for verification and limitations by noting the voltage transfer characteristics. The model, shown in figure 5, absorbs the effects of the link winding into the primary and secondary coils as illustrated, and as seen in equations (a), (b), and (c).[1]

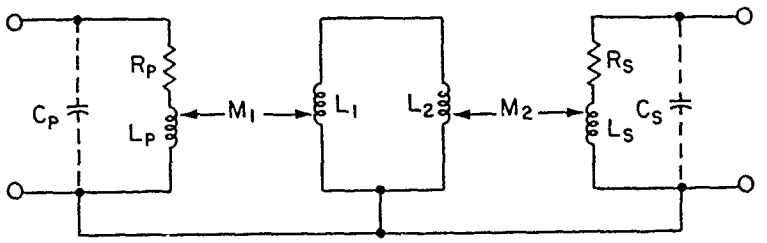

Figure 4. Simplified link coupled circuit.

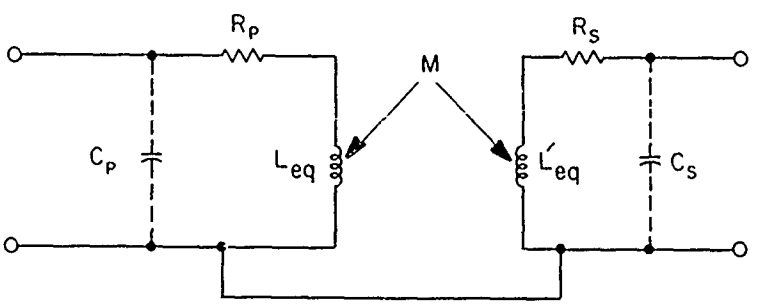

where

$$L_{eq} = L_p - \frac{M_1^2}{L_1 + L_2} \quad (a) \qquad L'_{eq} = L_S - \frac{M_2^2}{L_1 + L_2} \quad (b)$$

and

$$M = \frac{M_1 M_2}{L_1 + L_2} \quad (c)$$

where M_1, M_2, L_1, L_2, L_p and L_S are from figure 4.

Figure 5. Working model of the equivalent circuit.

---

[1] *Frederick E. Terman, Radio Engineers Handbook (McGraw-Hill, N.Y. 1943), p. 128.*

3. PHYSICAL RATIONALE FOR MODEL

Although an exact, general model for the inductively-coupled system was determined to be impracticable to develop at present, some attempt at a qualitative explanation seems appropriate.†

The principles of operation for the model rationale were determined by an intuitive reasoning, application of Faraday's induction law, which states that a changing magnetic field will produce an electromotive force and Lenz's law, which states that the direction of an induced emf is such as to oppose the cause producing it.[3] The important fact is that energy is inductively coupled from the sending coil to the receiving coil in useful quantity, notwithstanding the conducting shield effect of the intervening rocket tube, when the rocket tube is slotted.

From Faraday's induction law, it is seen that an emf and current will be induced in the rocket tube when an ac voltage is applied to the sending coil. The induced current in the rocket tube will flow parallel to the turns of the sending coil and generate a magnetic field in opposition to the magnetic field of the sending coil. This effect reduces the number of effective flux linkages through the sending coil and subsequently the receiving coil. The effects of reduced flux linkages are manifested by a reduction of the sending coil self-inductance from that of the air core case. More importantly, for the remote set application, coupling between the sending and receiving coils is reduced, since inductance and mutual inductance are both directly proportional to the number of flux linkages produced by the current in the sending coil. Referring to figure 3, where the link circuit is the only portion of the circuit derived somewhat unconventionally, the operation is summarized as follows: The inductive coupling M_1 represents the measure of inductive coupling between the sending coil and the rocket tube (see fig. 5). It tends to reduce the effective sending coil inductance L_{eq} since,

$$L_{eq} = L_p - \frac{M_1^2}{L_1 + L_2}.$$

The inductive coupling factor M_2 represents the energy exchange between the rocket tube and receiving coil. It results (as explained below) from the current flowing around the slot. The direct, inductive coupling between the sending coil and receiving coil is effected by the relatively few linkages through the rocket tube represented by M_3.

---

†*See appendix B for a suggested approach to a theoretical solution.*

[3]*Sears and Zemansky, University Physics Part 2, Electricity and Optics (Addison-Wesley Press, 1952).*

The factor M_3 is negligible because of the conducting shield effect, which attenuates the energy by 8.69 a/d dB where a/d is the ratio of the conductor thickness to the skin depth[4] (the distance from the surface at which the current density has dropped by 63.2 percent). For the configuration under study: an aluminum rocket tube with a = 0.052 in. wall thickness at about 150 kHz giving a skin depth of d = 0.009 in., the predicted attenuation is greater than 50 dB.

When one or more slots are cut parallel to the axis common to the coils and rocket tube, the flux linkages affecting the sending coil inductance

$$\left(L_{eq} = L_P - \frac{M_1^2}{L_1 + L_2} \right)$$

and the sending coil to receiving coil mutual inductance

$$\left(M = \frac{M_1 \, M_2}{L_1 + L_2} \right)$$

are increased (see fig. 5). A reasonable physical conception of the slot effect can be obtained with the aid of figure 6.

The current induced in the rocket tube I_{RT} is represented by six "current filaments," which normally would flow parallel to the sending coil (perpendicular to the length of the slot). As they approach the slot they divide into two equal groups of three current filaments. The currents then flow around the slot. Techniques for the mapping of fluid flow (which is analogous to current flow)[5] indicate a bunching of the current filaments as they pass by the slot. The magnetic intensity vector H_D, resulting from the current flowing by the slot, causes flux linkages between the rocket tube and the receiving coil, thereby overcoming the conductive shieldin effect. The quantity M_2 and consequently,

$$M = \frac{M_1 \, M_2}{L_1 + L_2}$$

is influenced by H_D. Magnetic intensity vectors H_A, H_B and H_C are used to help illustrate the effect of the curving current filaments on the sending coil inductance L_{eq}. The implication is that the reduction in

---

[4] *Frederick E. Terman, Electronic and Radio Engineering, (McGraw Hill, 1955), p. 36.*

[5] *Walter E. Rogers, Electric Fields (McGraw Hill, 1954).*

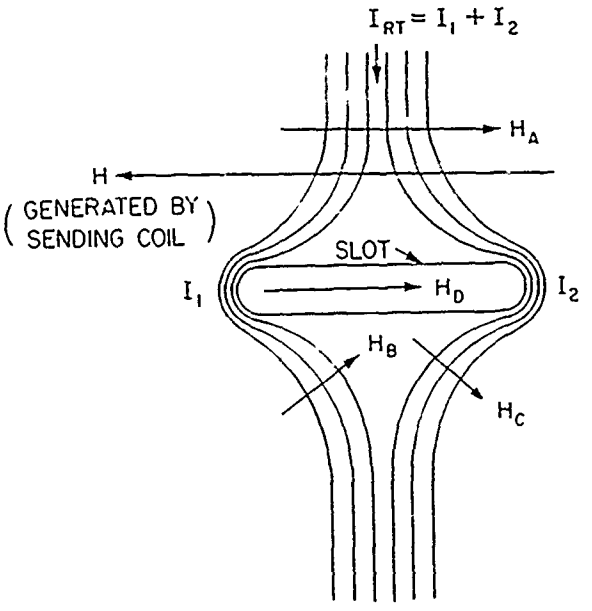

Figure 6. Magnetic intensity vectors and current flow model around slot.

L_{eq} is not as great as it would be with noncurving filaments (i.e., without the slot) since cancellation of flux lines from the sending coil is not as great with current filaments curving around the slot. It will also be noted that with the slot, M_1 is decreased (because of the misalignment of H with H_B and H_C) and

$$L_q = L_p - \frac{M_1 M_2}{L_1 + L_2}$$

indicates an increase in L_{eq}. Measurements show a 20-percent increase (from 2.5 to 3.0 μH), in L_{eq} measurement after introducing a slot in the rocket tube. Measurements also show an increase of more than 20 dB in (the overall coupling coefficient) M after the slot is introduced. From this it is apparent that the effect of the increase in M_2 more than compensates for the decrease in M_1, since,

$$M = \frac{M_1 M_2}{L_1 + L_2}.$$

When the number of slots was increased from one to two to four, there was a corresponding increase in M by factors of 1 (reference) to 1.45 to 1.88 respectively, which suggests a possible linear relationship between M and the number of slots. Widening the vertical dimension of a single slot from 0.030 to 0.475 in. increased M by a factor of 1.64. Since only two widths were tried, no relation other than an increase in M is suggested by the results at present. Neither is there a good

basis for a relation between number of slots and slot width on the effect of M. The effect of slot length was shown in a previous investigation at HDL* to increase M with increasing slot length. In order to obtain better relationships on the effect of slot physical characteristics, another experiment or a mathematical solution of the boundary value problem would be necessary.

4. VERIFICATION OF MODEL

The following procedure was used to verify the model. First, the key circuit operation parameters (E_{out}/E_{in}, M) and electrical elements (R, C, and L) were identified. Next, the necessary simplifying assumptions were made as described in the development of the working equivalent circuit. Measurements of the quantities involved were then made using the physical circuit configuration. Finally, the model was exercised by varying certain quantities and observing the originally measured and calculated values for consistency.

The assumed circuit element values of R_p, L_{eq}, R_S, L'_{eq} and C_S were determined using the test techniques outlined in appendix A. The value of C_p was found to be negligibly small and in any event was eliminated as a consequence of the low impedance (approximately 2 Ω) voltage source placed across it at the input of the sending coil. An equivalent circuit derived from figure 5, and shown in figure 7, can be used in describing the verification procedure.

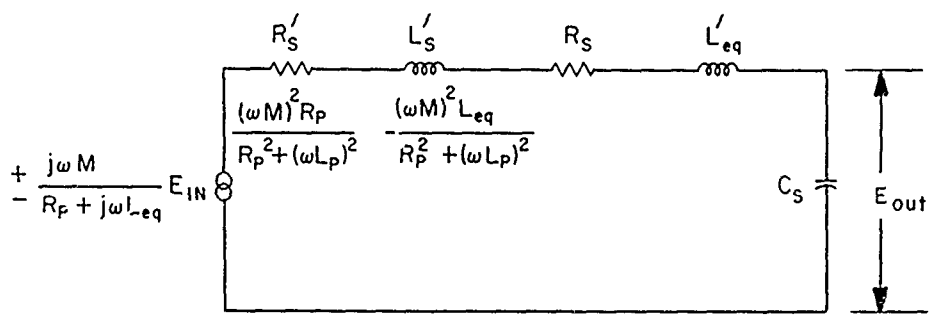

Figure 7. Equivalent output circuit.

As a result of the relatively low coupling between input and output circuits, R'_S and L'_S in figure 7 were found to be negligible. The value of M was calculated from measurements of E_{out}/E_{in} (complex) at its peak

*This investigation was made by Edward T. Spielman at the Harry Diamond Laboratories.

magnitude, which occurred at about 182 kHz, and equation (1) which was derived from figure 7 with R_S' and L_S' set to zero.

$$M = \left(E_{out}/E_{in}\right) \times \left[R_P + j\omega L_{eq}\right] \times \omega C_S \left[R_S + j\left(\omega L_{eq}' - 1/\omega C_S\right)\right]. \qquad (1)$$

Measurements and calculations were then made at other frequencies and with several different values of external capacitance to show constancy in the value of M. At frequencies between 100 and 200 kHz the magnitude of M stayed within 15 percent of 1 μH at phase angles between 182 and 195 deg (as shown in table I).

Ideally, M should be constant and real (i.e., the phase angle should be 0 or 180 deg, depending on the terminal connection polarity). This requirement has been reasonably met (with a bias of about +10 deg in phase angle) considering the possibilities for error accumulation when applied to the several electrical quantities measured. See appendix A for measurement techniques and table I for the effects of slight variation in some of the measured values on the magnitude and phase angle of the calculated mutual inductance.

Arbitrarily fixing the value of M at 0.89 μH (the average value of M calculated at E_{out}/E_{in} max), calculations of E_{out}/E_{in} (magnitude and phase) were made over a range of frequencies between 110 and 200 kHz using equation No. (1), and compared with a corresponding set of measured values taken with C_S constant at 225 pF (the sum of the receiving circuit distributed capacitance and phase meter capacitance). The calculated values of E_{out}/E_{in} (phase and magnitude) were again close enough to verify the model (see fig. 8) for the calculated versus measured values of the magnitude response and figure 9 for the phase response.

The values of M_1, M_2, L_1, and L_2 were indeterminate using the methods described herein. In order to determine these values and thus completely describe the equivalent circuit of figure 4, either the boundary value problem described in appendix B must be solved, or more involved test techniques will have to be developed to extract the undetermined values. The working model is useful, however, as described in section 5.

5. APPLICATION OF THE EQUIVALENT CIRCUIT

The equivalent circuit developed (see fig. 4) can be used as a qualitative design aid in understanding the effects of external circuit changes on the voltage transfer characteristics. With some limitations, quantitative effects can be predicted using the working model of figure 5. As an example, the input loading effects can be predicted once the circuit elements (fig. 5) are known. Similarly, the output frequency reponse can be calculated with the additional knowledge of the load impedance connected across C_S.

TABLE I. MUTUAL INDUCTANCE CALCULATION RESULTS

Reference values (Mean value of M @ E_{out}/E_{in} max, M + 0.89 μH)						Sensitivity calculations								
Frequency (kHz)	R_S (Ω)	C_S (pF)	E_{out}/E_{in} (dB)	M* (μH)	M* (deg)	C_S' variation	M** (μH)	M** (deg)	R_S' variation	M** (μH)	M** (deg)	E_{out}/E_{in} variation	M** (μH)	M** (deg)
180 f_o	1050	225	-1.1	0.83	195	$C_S' = 1.05\ C_S$	0.89	205	$R_S' = 1.05\ R_S$	0.87	194	0.5 dB + E_{out}/E_{in}	0.88	195
204 $f_{-3\ dB}$	1050	225	-4.1	0.91	194									
165 f_o	965	225	-1.1	0.82	191	$C_S' = 1.05\ C_S$	0.89	201	$R_S' = 1.05\ R_S$	0.87	191	0.5 dB + E_{out}/E_{in}	0.88	191
187 $f_{-3\ dB}$	965	225	-4.1	0.91	192									
153 f_o	900	314	-0.5	0.90	193	$C_S' = 0.95\ C_S$	0.86	182	$R_S' = 0.95\ R_S$	0.86	193	E_{out}/E_{in} -0.5 dB	0.85	193
173 $f_{-3\ dB}$	900	314	-3.5	0.94	190									
144 f_o	850	359	-0.5	0.92	190	$C_S' = 0.95\ C_S$	0.87	179	$R_S' = 0.95\ R_S$	0.88	191	E_{out}/E_{in} -0.5 dB	0.87	191
164 $f_{-3\ dB}$	850	359	-3.5	1.07	189									
111 f_o	660	590	+0.2	0.98	186	$C_S' = 0.95\ C_S$	0.95	175	$R_S' = 0.95\ R_S$	0.94	186	E_{out}/E_{in} - 0.5 dB	0.92	186
128 $f_{-3\ dB}$	660	590	-2.8	1.17	182									

**M values calculated from actual measurements*
***M values calculated using changes in the indicated parameter*

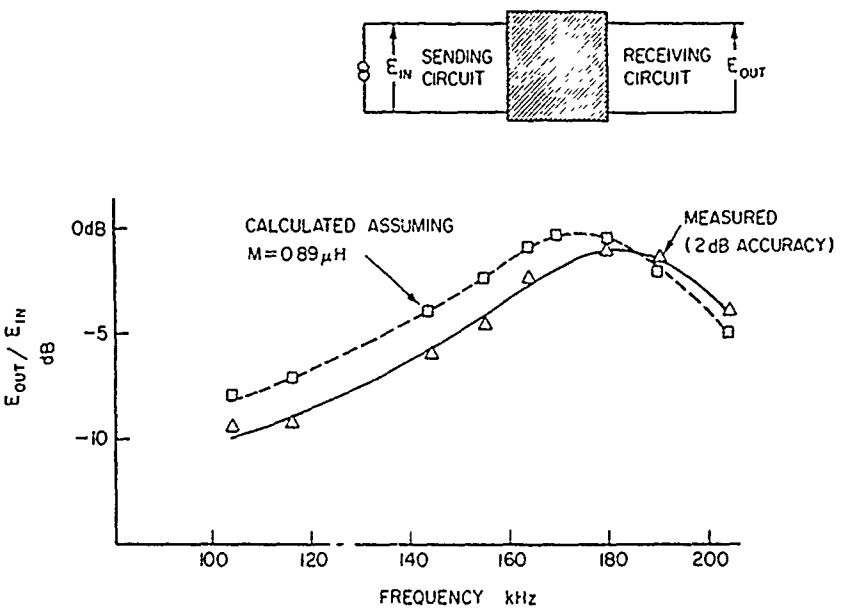

Figure 8. Calculated versus measured values of $|E_{out}/E_{in}|$

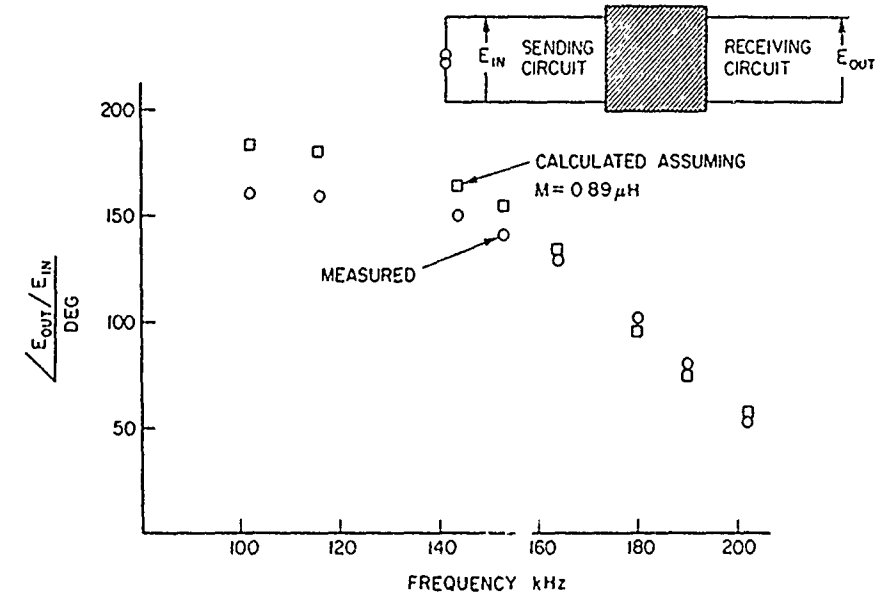

Figure 9. Calculated versus measured values of E_{out}/E_{in} phase.

Knowledge of the equivalent circuit configuration will aid in making judgments regarding sending and receiving circuit design goals. For example, the effects of double tuning techniques on bandwidth can be assessed. Unfortunately, much of the design would be empirical because equations cannot be used to obtain an initial "paper" design. This is true because analytical solutions for the "conducting shield" effects on inductances and coupling are unavailable at this time.

However, empirical design techniques can be used in combination with the equivalent circuit knowledge to accomplish a design. As an example, the sending coil can be designed by constructing several coils with the same configuration (e.g., single layer of No. 20 AWG copper wire) but with each coil having a different number of turns.* The values of L_{eq}, C_p, R_p and M can then be determined experimentally for each of the coils and curves plotted. The resulting parametric plots can be interpolated to predict the characteristics of coils with intermediate numbers of turns. The equivalent circuit (fig. 5) can then be used to predict loading and frequencyresponse characteristics. Other parameters would, of course, need to be investigated in a similar manner to completely optimize the coupling system. Some other prominent parameters would be slot dimensions and frequency of operation.

6. CONCLUSIONS

An appreciable amount of electrical energy can be inductively coupled from a coaxially wound coil into an electrically conducting rocket tube when a slot is cut in the tube surface parallel to the cylindrical axis. By consideration of Faraday's law of induced emf, and Kirchoff's and Ohm's laws of current flow, it is seen that currents induced in the rocket tube by the sending coil's magnetic field flow in directions around the slot, creating a magnetic field that links the turns of the receiving coil inside the rocket tube. The "slot magnetic field," compared with the magnetic field from the currents in the rocket tube surface, is relatively unaffected by the conducting-shield effect of the rocket tube. These considerations suggest a three-coil tandem, coupled (inductive) circuit as a basic model. When the equivalent electrical parameters of the circuit are measured, the input-output characteristics of the coupling system are predictable. Thus, a basic explanation of the coupling operation and a design aid are available for the inductively coupled remote set fuzing configuration.

To obtain a more generalized analytical solution of the problem, an extended effort must be made using boundary value solutions to Maxwell's equations.

---

*This procedure was suggested by Ralph G. Moore of HDL.

LITERATURE CITED

(1) Frederick E. Terman, Radio Engineers Handbook (McGraw Hill, N.Y., 1943).

(2) Joint Munitions Effectiveness Manual, Air-to-Surface Weapons Characteristics Handbook (JMEM) Change 5, 29 December 1972.

(3) Sears and Zemansky, University Physics Part 2, Electricity and Optics (Addison-Wesley Press, 1952).

(4) Frederick E. Terman, Electronic and Radio Engineering (McGraw Hill, N.Y., 1955).

(5) Walter E. Rogers, Electric Fields, (McGraw Hill, 1954).

SELECTED BIBLIOGRAPHY

Electronic Measurements, Second Edition, Terman & Pettit, McGraw Hill Inc., (1952).

Radiotron Designers Handbook, Fourth Edition, Langford-Smith, published by Wireless Press for Amalgamated Wireless Value Company PTY. LTD. 47 York Street, Sydney, Australia, (1953).

Electrical Engineering Circuits, Second Edition, Skilling, Wiley, (1965).

Circuits, Matrices and Linear Vector Space, Huelsman, L.P., McGraw Hill, Inc., (1963).

The Theory and Design of Inductance Coils, Welsby, V.G., McDonald & Co. London, (1950).

ACKNOWLEDGMENT

I wish to thank O.R. Cruzan who authored appendix B and offered helpful suggestions in determining the creation of the slot magnetic fields.

APPENDIX A--MEASUREMENT TECHNIQUES

A-1. Measurement Objectives

The methods and techniques used to extract the circuit quantities were sufficiently peculiar to warrant documentation for future reference. The object of the measurements was to identify the circuit element values of the equivalent circuit working model (sect 3, fig. 5) and to use them in further measurements to verify the accuracy of the model.

Figure A-1 is a schematic representation of the coupling system from which the measurement philosophy can be examined.

Most of the measurements were made with a Hewlett-Packard 3575A-type phase meter and a frequency counter.

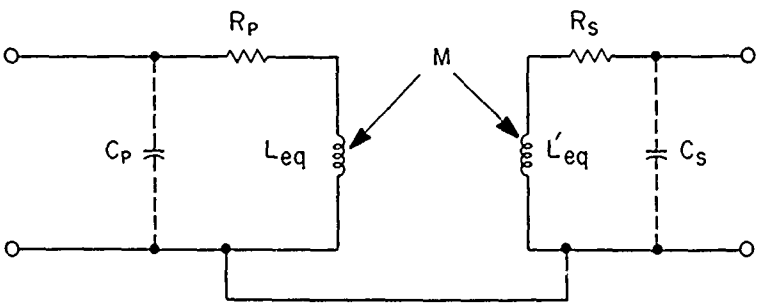

Figure A-1. Schematic diagram of the coupling system.

A-2. Sending Circuit Measurements

$$\left(L_{eq},\ R_P\right)$$

The primary measurements L_{eq} and R_P where L_{eq} consists of the inductive effects of the sending coil, intrinsic inductance were made using the connection shown in figure A-2.

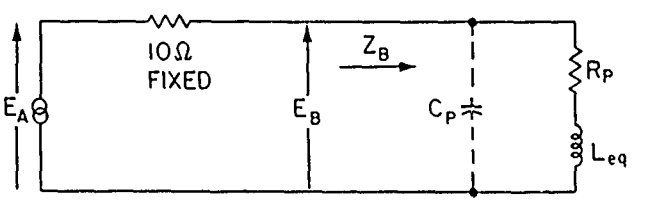

Figure A-2. Primary measurement circuit.

First, C_p was determined to have negligible effect by determining $Z_B = \left[E_B/\left(E_B - E_A\right)/10\right]$ and noticing that for frequencies in the range of interest (between 100 and 200 kHz) determined by the self-resonant frequency (182 kHz) of the receiving coil circuit, $Im(Z_L)/2\pi f$ was constant at 3.5 μH, so that L_{eq} was set to 3.5 μH. $Re(Z_B)$ was constant at approximately 0.5 Ω, so that R_p was set to 0.5 Ω.

A-3. Receiving Circuit Measurements

$$\left(L'_{eq},\ C_S,\ R_S\right)$$

The receiving circuit quantities were obtained using the connection of figure A-3 by connecting several (theoretically, only two are necessary)[1] values of external capacitance C_x across the receiving circuit output terminals and adjusting signal generator frequency to resonance by maximizing E_{out}. Coupling energy into the receiving circuit by induction is equivalent to placing a generator in series with the inductance, resistance and distributed capacitance of the receiving circuit so that series resonance was accomplished. It is important to use series rather than parallel resonance (commonly used) for a direct estimate of the elements L'_{eq} and C_S since, in this case, the circuit Q of the receiving circuit was less than 10 (approximately 3.5 because of the eddy current effect of the fuze base) where the peak voltage and zero power factor do not occur at the same frequency. This low Q situation would invalidate the technique used here for a parallel circuit where the approximation that $\omega_o^2 = 1/(LC)$ holds for Q around 10 or more. The distributed capacitance C_S was then calculated using equation (A-1).

$$C_S = \frac{C_2(f_2/f_1)^2 - C_1}{\left[1 - (f_2/f_1)^2\right]} \qquad \text{(A-1)}$$

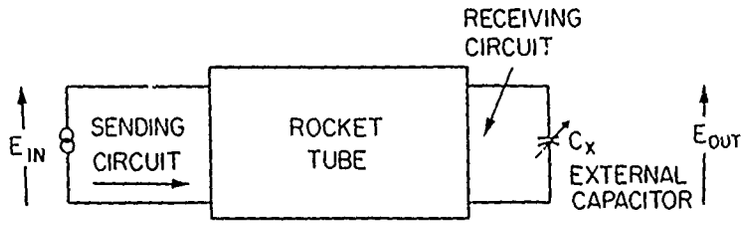

Figure A-3. Connection for measurements of L'_{eq} and C_S.

[1] *Electronic Measurements, Second Edition, Terman & Pettit, McGraw-Hill Book Inc., (1952) p 100.*

The inductance L'_{eq} was then calculated from,

$$L'_{eq} = 1/\left[4\pi^2 f_1^2 (C_1 + C_S)\right] \qquad \text{(A-2)}$$

where C_1, C_2 are any two values of external capacitance and f_1 and f_2 are the corresponding resonant frequencies.

Theoretically, L'_{eq} would be expected to vary from the effect of the eddy currents induced in the aluminum fuze base around which the receiving coil was wound, by a factor of $-M^2_{RF}/L_{FB}$, which is the effective inductance reflected into the coil from the fuze base. M_{RF} is th mutual inductance between the receiving coil and fuze base and L_{FB} the fuze base inductance. The experimental data resulting from equation (A-2), however, show the inductance to be practically constant at L'_{eq} = 3.5 mH throughout the frequency range. The distributed capacitance thus determined was 192 pF when the output capacitance of the phase meter (measured independently) of 33 pF was acounted for. The 33 pF was of necessity connected across the 192 pF of distributed capacitance throughout the tests, so that the minimum value of C_S was 225 pF with the phase meter connected.

The receiving circuit resistance R_S is a function of frequency because of eddy currents and proximity effect within the 500-turn winding of AWG No. 39 wire. The connection used to determine R_S as a function of frequency is shown in figure A-4.

The procedure involved adjusting C_X to obtain $Im(Y_B) = 0$ (i.e., parallel resonance) at several frequencies in the 114-to 188-kHz range. This was accomplished in each case by adjusting the frequency of the signal generator so that the phase angle of E_B was zero.

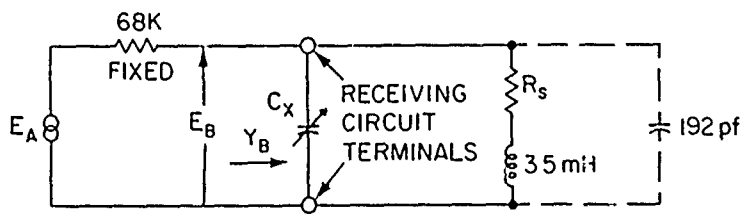

Figure A-4. Connection for determining R_S.

The following relationships were then used to determine R_S:

$$Y_B = Y_S + Y_C \tag{A-3}$$

$$Y_S = 1/\left(R_S + j\omega L\right) \tag{A-4}$$

$$= R_S/\left[R_S^2 + \left(\omega L\right)^2\right] - j\omega L/\left[R_S^2 + \left(\omega L\right)^2\right]$$

where $L = L'_{eq} = 3.5$ mH, as described above. At parallel resonance,

$$\omega L/\left[R_S^2 + \left(\omega L\right)^2\right] = \omega\left(C_S + C_X\right) \tag{A-5}$$

so that

$$Y_B = Y_S \ ,$$

(i.e., since the sum of the imaginary components of $Y_B = 0$)

and

$$\left[R_L^2 + \left(\omega L\right)^2\right]/R_S = Z_B \tag{A-6}$$

but,

$$Z_B = 68\ K\ \left(E_B/E_A\right)/\left[1 - \left(E_B/E_A\right)\right] \ . \tag{A-7}$$

Note at resonance E_B/E_A is real.

Then, multiplying the results of equations (A-5) and (A-6),

$$\left|\omega L/\left[R_S^2 + \left(\omega L\right)^2\right]\right| \times \left|\left[R_S^2 + \left(\omega L\right)^2\right]/R_S\right| = \omega C\ Z_B \ , \tag{A-8}$$

where $C = C_S + C_X$ gives

$$R_S = \omega L/\omega C Z_B \ , \tag{A-9}$$

or

$$R_S = L_S/\left\{C \cdot 68\ K\ \left(E_B/E_A\right)/\left[1 - \left(E_B/E_A\right)\right]\right\} \ .$$

The values of R_S were plotted at several points in frequency. Other values of R_S throughout the frequency range were taken from a straight-line fit through the points. The straight-line approximation was later justified by the consistency of the results of the mutual inductance and voltage transfer (E_{out}/E_{in}) calculations.

A-4. Voltage Transfer Measurements E_{out}/E_{in}

The voltage transfer measurements E_{out}/E_{in} were obtained with the connection in figure A-3. The measurement accuracy of the Hewlett-Packard 3575A phase meter was approximately 2 dB for the E_{out}/E_{in} measurement and 5 degrees for the phase angle measurements.

APPENDIX B--NUMERICAL SOLUTION OF AN ELECTROMAGNETIC PROBLEM

By O. R. Cruzan

In general, the determination of the diffraction field of a perfectly conducting body located near a primary electromagnetic source presents almost insurmountable analytical difficulties. These arise, in some cases, from the number of boundaries on which boundary conditions must be satisfied, the number of partial fields that must be related to each other, and, in other cases, to the gross irregularities of the surface.

An alternate method of solving such problems is by what is known as a theoretic-numeric technique. This method has proven successful for bodies of various sizes and shapes.[1,2,3,4] In this method the surface of the body is subdivided by a grid system. The surface current over each elemental area or grid is assumed to be uniform.

Now, the magnetic field produced by a surface current is given by the formula,

$$\bar{H}_S = \frac{1}{4\pi} \int_S \nabla \times \left(\bar{J}_s \frac{e^{-jkr}}{r} \right) ds \qquad \text{(B-1)}$$

Alternatively, this formula can be written as

$$\bar{H}_s = \frac{1}{4\pi} \int_S f(r) \quad \bar{J}_s \times i_r \, dS \qquad \text{(B-2)}$$

where

$$f(r) = - \left(\frac{1}{r^2} + j \frac{k}{r} \right) e^{-jkr}. \qquad \text{(B-3)}$$

---

[1] *R.L. Tanner and M.G. Andreason, "Numerical Solution of Electromagnetic Problems," IEEE Spectrum, 4, No. 9 (1967), pp 53-61.*

[2] *F.K. Oshiro, K.M. Mitzner and R.G. Cross, "Scattering From Finite Cylinders by Source Distribution Techniques," Proc. of GISAT Symposium (2nd) vol II, Oct (1967), pp 57-70.*

[3] *J. Goldhirsh, D.L. Knepp and R.J. Doviak, "Radiation From a Dipole Near a Conducting Cylinder of Finite Length," IEEE Trans on Electromagnetic Compatability, EMC-12, No. 3, Aug (1970), pp 96-105.*

[4] *A.H. Cherin and J. Goldhirsh, "Impedance and Far Field Characteristics of a Linear Antenna Near a Conducting Cylinder," IEEE Trans on Electromagneti Compatibility, EMC-14, No. 3, Aug (1973), pp 110-117.*

In these formulas $\bar{H}_s$ is the scattered field, $\bar{J}_s$ is the surface current, r is the distance from the current $\bar{J}_s$ to a point of observation, i_r is a unit vector whose direction is parallel to that of $\bar{r}$, k is the propagation constant of free space, S is the total surface area of the scattering body, and dS is the differential of surface area.

Let $\bar{H}_s'$ be the total scattered magnetic field due to the surface current $\bar{J}_s'$, except for that of an elemental area. The magnetic field in space $\bar{H}_t'$ is the sum of the primary field $\bar{H}_p$, due to the source, and the scattered field $\bar{H}_s'$, due to the surface current $\bar{J}_s'$. Thus,

$$\bar{H}_t' = \bar{H}_p + \bar{H}_s' \quad . \tag{B-4}$$

Now at the surface of the elemental area, $\bar{H}_t'$ will be the incident magnetic field. From a consideration of the electrogmagnetic fields in the presence of a conducting body, it can be shown that as the conductivitiy of the body becomes infinite, the tangential components of the incident and reflected magnetic fields at the surface become equal; that is,

$$\hat{n} \times \bar{H}_s = \hat{n} \times \bar{H}_t' \quad . \tag{B-5}$$

The boundary condition for the magnetic field at the surface of a perfect conductor is

$$\hat{n} \times \left(\bar{H}_t' + \bar{H}_s = \bar{J}_s'\right), \tag{B-6}$$

where $\hat{n}$ is the unit vector normal to the surface. In view of equation (B-5) we get from equation (B-6)

$$\hat{n} \times \bar{H}_t = \bar{J}_s/2 \quad , \tag{B-7}$$

since $\bar{H}_t' \to \bar{H}_t$ and $\bar{J}_s' \to \bar{J}_s$, as the elemental area approaches zero.

Using equations (B-2) and (B-4) with (B-7), we get

$$\hat{n} \times \left[\bar{H}_p + \frac{1}{4\pi} \int_S f(r)\ \bar{J}_s \times i_r\ dS\right] = \frac{\bar{J}_s}{2} \quad . \tag{B-8}$$

If we denote by i the number of the grid at whose center the surface current is to be determined, and by n the number of a source grid, then, in view of the assumption of uniform current over a grid, the integral in equation (B-8) may be replaced by a summation; thus we get

$$\hat{n}_i \times \left(\sum_{n=1}^{n} H_{in} \right) - \frac{\bar{J}_i}{2} = - \hat{n}_i \times \bar{H}_{pi}, \qquad i = 1,2,3 \ldots N \qquad \text{(B-9)}$$

where

$$\bar{H}_{in} = \frac{1}{4\pi} \int_{S_n} f(r_{in}) \, \bar{J}_n \times i_{rin} \, dS_n \, . \qquad \text{(B-10)}$$

Here

$\hat{n}_i$ is the normal unit vector at the center of the ith grid,

$\bar{H}_{pi}$ is the primary field at the center of the ith grid,

$\bar{J}_i$ is the surface current density at the center of the ith grid,

$\bar{J}_n$ is the surface current density at the center of the nth grid,

r_{in} is the distance from a point of the nth grid to the center of the ith grid,

i_{rin} is the unit vector having the direction of $\bar{r}_{in}$,

$f(r_{in})$ is the function given in equation (B-3) connecting grids i and n,

S_n is the area of the nth grid.

Since the surface current over each grid may be decomposed into two orthogonal components, then equation (B-9) results in 2 N simultaneous equations in 2 N unknowns--the unknowns being the surface current components over the grids.

After the J_n's have been determined, equation (B-1) is used to obtain the scattered field. This field, together with the primary field, combined according to equation (B-4), gives the total magnetic field at a point of observation.

A problem for which the theoretical-numerical technique may be applicable is that of a perfectly conducting tube of finite length containing an axial slot. The primary electromagnetic field is provided by a circular, current-bearing loop. The loop and the tube are coaxial. This system is illustrated in figure B-1. Also illustrated in the same figure are a grid system that is appropriate to the technique, and several of the elements involved in the evaluation of the field. These elements are the surface current $\bar{J}_n$ at the center of the nth grid, the distance r_{in} from the center of the nth grid to a point of the ith grid, the unit vector i_{rin} that is parallel to the direction of $\bar{r}_{in}$, and the unit vector $\hat{n}_i$ that is normal to the surface at the center of the ith grid. The dots in the centers of the grids indicate the positions at which the surface currents are to be determined.

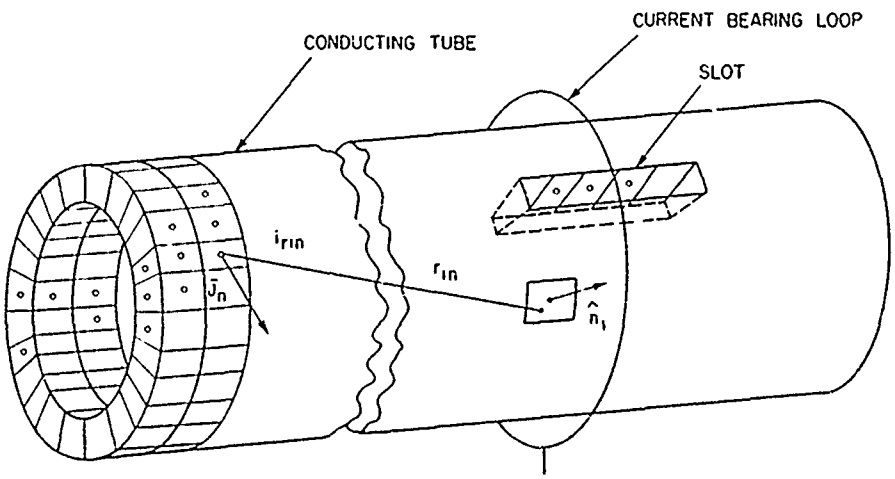

Figure B-1. Grid system for theoretic-numeric technique.

DISTRIBUTION

DEFENSE DOCUMENTATION CENTER
CAMERON STATION, BUILDING 5
ALEXANDRIA, VA 22314
ATTN DDC-TCA (12 COPIES)

COMMANDER
US ARMY MATERIEL COMMAND
5001 EISENHOWER AVENUE
ALEXANDRIA, VA 22333
ATTN AMCDL, DEP FOR LABORATORIES
ATTN AMCRD, DIR RES, DEV, & ENGR

COMMANDER
USA MISSILE COMMAND
REDSTONE ARSENAL, AL 35809
ATTN AMSMI-R, RDE & MSL DIRECTORATE
ATTN OFFICE OF THE PROJ MGR FOR
2.75-INCH ROCKET SYS

COMMANDER
USA ARMAMENTS COMMAND
ROCK ISLAND, IL 61201
ATTN AMSAR-ASF, FUZE DIV
ATTN AMSAR-RDC, CONFIG MGMT DIV
ATTN AMSAR-RDF, SYS DEV DIV - FUZES

OFC, CHIEF OF RESEARCH & DEVELOPMENT
USA RSCH & DEV GROUP (EUROPE)
BOX 15
FPR NEW YORK 09510
ATTN LTC EDWARD E. CHICK
CHIEF, MATERIALS BRANCH

COMMANDER
USA MISSILE & MUNITIONS CENTER & SCHOOL
REDSTONE ARSENAL, AL 35809
ATTN ATSK-CTD-F

COMMANDER
USA WEAPONS COMMAND, HQ
ROCK ISLAND, IL 61201
ATTN SWERR-PL, TECHNICAL LIBRARY

COMMANDING OFFICER
NAVAL AVIONICS FACILITY
6100 E. 21 STREET
INDIANAPOLIS, IN 46218
ATTN LIBRARY (ADL)

COMMANDER
NAVAL SURFACE WEAPONS CENTER
WHITE OAK, MD 20910
ATTN CODE 730, LIBRARY DIV

COMMANDER
NAVAL ORDNANCE STATION
INDIAN HEAD, MD 23680
ATTN CODE GS-73

COMMANDER
NAVAL WEAPONS CENTER
CHINA LAKE, CA 93555
ATTN CODE 457, PROPULSION SYS DIV

COMMANDER
NAVAL SURFACE WEAPONS CENTER
DAHLGREN, VA 22448
ATTN G
ATTN GA
ATTN GB
ATTN GP
ATTN GW
ATTN GW (AIDS)

DIRECTOR
US MARINE CORPS LANDING FORCE DEV CENTER
MARINE CORPS SCHOOLS
QUANTICO, VA 22134
ATTN GROUND OPERATIONS

COMMANDER
ARMAMENT DEVELOPMENT AND TEST CENTER
EGLIN AIR FORCE BASE, FL 32542
ATTN DLD, GUNS & ROCKETS DIV

COMMANDER
US ARMY MATERIEL COMMAND
REDSTONE ARSENAL, AL 35809
ATTN AMCPM-RK

OFFICE, CHIEF OF RESEARCH, DEVELOPMENT,
AND ACQUISITION
DEPARTMENT OF THE ARMY
WASHINGTON, DC 20310

EMERSON ELECTRIC COMPANY
8100 W. FLORISSANT
ST LOUIS, MO 63136
ATTN EMERSON ELECTRONICS &
SPACE DIV, STEVE LIFWICKI,
SENIOR STAFF ENGR

COMMANDER
NAVAL SEA SYSTEMS COMMAND
2521 JEFFERSON DAVIS HIGHWAY
ARLINGTON, VA 20360
ATTN NORD-035C1
ATTN NORD-55GA
ATTN NORD-55Z

DISTRIBUTION (CONT'D)

HARRY DIAMOND LABORATORIES
ATTN EINSEL, DAVID W., COL, COMMANDING
OFFICER/FLYER, I.N./LANDIS, P. E./
CONRAD, E.E./SOMMER, H.
ATTN CARTER, W.W.,DR., ACTING TECHNICAL
DIRECTOR/MARCUS, S.M.
ATTN KIMMEL, S., PIO
ATTN CHIEF, 0021
ATTN CHIEF, 0022
ATTN CHIEF, LAB 100
ATTN CHIEF, LAB 200
ATTN CHIEF, LAB 300
ATTN CHIEF, LAB 400
ATTN CHIEF, LAB 500
ATTN CHIEF, LAB 600
ATTN CHIEF, DIV 700
ATTN CHIEF, DIV 800
ATTN CHIEF, LAB 900
ATTN CHIEF, LAB 1000
ATTN RECORD COPY, BR 041
ATTN HDL LIBRARY 3 COPIES
ATTN CHAIRMAN, EDITORIAL COMMITTEE 4 COPIES
ATTN CHIEF, 047
ATTN TECH REPORTS, 013
ATTN PATENT LAW BRANCH, 071
ATTN MCLAUGHLIN, P. W., 741
ATTN DANNER, B., 440 (5 COPIES)
ATTN GOODMAN, R., 440
ATTN MANOLATOS, T., 440
ATTN PARKHURST, R., 120
ATTN TOZZI, L., 140
ATTN SAMBUCO, A. (10 COPIES)